Article

Compound Eye Morphology Revealed by SEM Enhances Species Discrimination in *Temnothorax* Ants (*Tuberum* Group)

Joaquín L. Reyes-López *

Posted Date: 3 April 2026

doi: 10.20944/preprints202604.0089.v1

Keywords: ocular morphology; setae; species delimitation; SEM; *Formicidae*

 doi:10.20944/preprints202604.0089.v1

Article

Compound Eye Morphology Revealed by SEM Enhances Species Discrimination in *Temnothorax* Ants (*Tuberum* Group)

Joaquín L. Reyes-López

Department of Botany, Ecology and Plant Physiology, Ecology Area, José Celestino Mutis Building, Rabanales Campus (C4), Carretera de Madrid Km 396, 14071 Córdoba, Spain; cc0relojl@uco.es

Abstract

The delimitation of cryptic species represents one of the main challenges, particularly in groups with low external morphological differentiation. In this context, scanning electron microscopy (SEM) enables the detection of diagnostic characters at the microscale. This study evaluates the potential of ocular morphology for interspecific discrimination within a group of species of the genus *Temnothorax*. A total of 246 workers from 52 nests, 13 populations, and 8 species from the Iberian Peninsula and North Africa were analyzed. Morphometric variables related to compound eyes were quantified from SEM images (ommatidia number, interommatidial setae, eye diameter). Data were analyzed using ANOVA, effect size estimation (η^2), Linear Discriminant Analysis (LDA), and Random Forest models. All variables showed significant differences among species ($p < 0.001$), with varying discriminative power. Variables related to ommatidial organization exhibited the highest classification performance, achieving high rates of correct species assignment in multivariate analyses. The use of nest-level means values substantially improved classification accuracy. These results demonstrate that ocular morphology analyzed through SEM represents a promising complementary tool for species discrimination in Temnothorax, complementing traditional and molecular approaches.

Keywords: ocular morphology; setae; species delimitation; SEM; *Formicidae*

1. Introduction

In taxonomy, alpha taxonomy refers to the traditional approach focused on the description, identification, and classification of organisms based on observable morphology, including species delimitation and the development of taxonomic keys. Despite its classical foundations, it is evolving through the integration of new technologies while maintaining a central role in biodiversity research, whose importance is expected to increase in response to the global biodiversity crisis. Currently, the field is advancing toward more integrative and data-driven approaches, incorporating tools such as DNA barcoding and digital imaging to improve species identification and description [1].

At its core, alpha taxonomy addresses the fundamental process of recognizing, describing, and naming species. Traditionally, this process has relied on observable morphological features; however, more recent approaches have expanded its scope through techniques such as X-ray–based analyses. In particular, soft X-ray tomography (SXT) allows the examination of internal cellular and tissue structures, facilitating species identification and characterization when conventional methods are insufficient [2].

Furthermore, recent advances in computational technology and microscopy have opened new possibilities for generating three-dimensional and interactive imaging [3]. Among these techniques are scanning electron microscopy (SEM), micro-computed tomography (micro-CT) [4], and synchrotron X-ray tomography [5]. These tools have the potential to revolutionize studies based on

 doi:10.20944/preprints202604.0089.v1

biological collections by enabling detailed analyses of both external and internal morphology in valuable or rare specimens without causing damage.

Scanning electron microscopy (SEM) is a highly valuable tool in alpha taxonomy, particularly for the detailed examination of surface features and structures that are difficult to resolve using light microscopy. Owing to its superior magnification and resolution, SEM enables precise characterization of traits such as surface sculpturing, fine appendage morphology, and other microstructural features of taxonomic relevance.

In the study of ants, SEM is especially useful for investigating external morphology, providing high-resolution images of exoskeleton. This includes detailed observation of structures such as setae, scales, and other surface ornamentations, as well as specialized appendages including antennae, legs, and mouthparts. Furthermore, SEM facilitates the analysis of ultrastructural features, such as cuticular layering and sensilla, which are critical for species delimitation and functional interpretation. SEM has been widely applied in myrmecological research, including the characterization of cuticular microstructures in *Strumigenys* [5], the analysis of mandibular cuticle morphology in *Atta* [7], and the description of spongiform bodies in *Strumigenys* [8].

Compound eyes are key sensory organs in insects, enabling visual perception finely tuned to their ecological and behavioral requirements. They are composed of multiple photoreceptive units known as ommatidia, each contributing a portion of the overall visual field and collectively providing panoramic vision with high sensitivity to motion and changes in light intensity [8]. This visual system is essential for critical behaviors such as foraging, predator avoidance, navigation in complex environments, and intraspecific visual communication [9]. Additionally, morphological variation in compound eyes may reflect ecological differences among species and can, in some cases, serve as a diagnostic character in taxonomic delimitation [2].

In ant systematics (taxonomy and phylogeny), ommatidia—the individual facets of the compound eye—are widely used as morphological characters due to their relative stability within species and variability across lineages subjected to different ecological pressures (e.g., subterranean lifestyles, nocturnality, or visually guided foraging). In practice, ommatidial counts are not performed as an end in themselves, but rather as a proxy for quantifying the degree of eye development.

Taxonomic studies rarely involve counting all ommatidia, particularly in species with large eyes. Instead, standardized metrics are typically employed, such as the number of ommatidia in the longest row or the maximum number of ommatidia across the eye, usually assessed in lateral or oblique view. These measurements are widely used in modern descriptions due to their repeatability using microscopy and digital imaging. In taxonomic revisions, they are commonly reported as “eyes with ~X ommatidia in the longest row.” Clear examples can be found in revisions of several genera and species complexes, such as *Tetramorium* [10], as well as in comparative diagnoses of hyperdiverse groups [11].

In other cases, ocular indices derived from standard morphometric measurements (e.g., eye length relative to head width) are employed, often in combination with ommatidial counts to provide an estimate of both eye size and functional “resolution.” In ant taxonomic literature, abbreviations such as EL (eye length) and OI (ocular index) are routinely used, frequently alongside ommatidial counts, particularly in species with reduced eyes [12]. As noted above, these characters are especially valuable in the diagnosis of cryptic species: when other morphological traits exhibit limited variation or overlap, eye size and structure—including ommatidial number—can provide reliable diagnostic features.

Moreover, these traits carry important ecological signal. Strongly reduced eyes or those with few ommatidia are typically associated with hypogean lifestyles or low-light microhabitats, whereas more developed eyes reflect a greater reliance on vision. Comparative studies on eye structure and ecology in ants have revealed consistent patterns across lineages and life-history strategies, which helps explain why these characters are effective not only for taxonomic diagnosis but also for ecological interpretation [13] (PLOS).

 doi:10.20944/preprints202604.0089.v1

In *Temnothorax* (Crematogastrini: Myrmicinae), ommatidial counts are a commonly employed character in regional revisions and clade-level studies, typically expressed as "X ommatidia in the longest row" and often accompanied by indices such as OI and EL. This approach is particularly informative in this genus, which comprises small-bodied species with relatively reduced eyes [14,15], where even slight differences in ommatidial number may carry diagnostic value.

Although not always strictly focused on systematics, studies in Temnothorax have also incorporated ommatidial counts in behavioral and biological contexts (e.g., asymmetry and lateralization [16]). Such work provides valuable insight into the actual range of intraspecific variation, including differences among castes and sexes, thereby offering an important contextual framework for taxonomic studies.

The primary aim of this study is to assess the value of compound eye structures and their immediate surrounding features as complementary characters for the delimitation of morphologically similar or cryptic species. We hypothesize that ocular morphology—particularly traits related to ommatidial organization and periocular structures—encodes a species-specific morphological signal that is partially independent of overall body size and provides additional discriminatory power beyond traditional morphometric characters. To this end, both the individual discriminatory power of these variables and their combined contribution in a multivariate framework are evaluated and compared with a set of traditional morphological variables commonly used in such studies. As a secondary objective, their applicability is explored across different species groups of Temnothorax within the same taxonomic complex.

2. Materials and Methods

Species Sampling

This study included several species of the genus *Temnothorax* belonging to the *tuberum* group (sensu [17]): *T. bejaraniensis* Reyes-López & Carpintero-Ortega, 2013 (=BEJ), *T. curtulus* (Santschi, 1929) (=CUR), *T. luteus* (Forel, 1874)(=LUT), *T. pardoi* (Tinaut, 1987)(=PAR), *T. racovitzai* (Bondroit, 1918)(=RAC), *T. tuberum* (Fabricius, 1775)(=TUB), and *T. unifasciatus* (Latreille, 1798)(=UNI).

To account for intraspecific geographic variation, most species were sampled from two or three geographically distant localities (in all cases separated by more than 50 km), except for *T. tuberum* and *T. unifasciatus*, for which only a single locality was available.

For *T. luteus*, two populations were compared: one from the Natural Park of the Sierras de Cazorla, Segura y Las Villas and another from the Sierra Mágina Natural Park, separated by approximately 60 km in a straight line. In *T. pardoi*, populations from the Sierras de Cazorla, Segura y Las Villas Natural Park and the Sierra de Guadarrama National Park were analyzed, with an approximate separation of 330 km. In the case of *T. curtulus*, three populations were included: two from Spain (Strait of Gibraltar region and Subbetic area), separated by approximately 200 km, and one from North Africa (Morocco). For *T. racovitzai*, populations from Sierra Morena and Sierra de Cardeña (central Andalusia, southern Spain) were compared, with a separation of approximately 60 km.

T. bejaraniensis was compared with a morphologically similar, yet undescribed species from the autonomous city of Ceuta (North Africa). Based on their morphological affinities, both forms can be assigned to the so-called "*tebesae* superspecies" [17], here treated as *T. tebesae* cfr (in *tebesae* complex) within the *tuberum* group. The distance between these populations is approximately 230 km, including a marine barrier. For *T. unifasciatus*, colonies were sampled from the Sierra de Guadarrama National Park, whereas *T. tuberum* specimens were collected in the Sierra de Albarracín (Teruel, Spain). Detailed information on the sampled material is provided in Table S1 of the supplementary material (Appendix A).

Preparation for Scanning Electron Microscopy (SEM)

Samples intended for scanning electron microscopy (SEM) require specific preparation procedures, including dehydration and coating with a conductive material (e.g., gold or carbon), to optimize imaging conditions. In this study, specimens were oven-dried at 60 °C for 48 h.

 doi:10.20944/preprints202604.0089.v1

Subsequently, the head of each worker was dissected and mounted on a metallic stub using a conductive adhesive (double-sided copper tape). Samples were then sputter-coated with a thin layer of gold to provide surface conductivity and enhance image quality. Only the head of each worker was prepared and mounted. For imaging and analysis, one side of the head was selected based on optimal orientation and preservation state (i.e., absence of debris, structural damage, etc.). When possible, measurements were also taken from the second eye of the same specimen.

Images were acquired using a JEOL JSM-6300 scanning electron microscope (JEOL Ltd., Tokyo, Japan). The instrument provides a high depth of field compared to optical microscopy, allowing detailed visualization of three-dimensional structures. Observations were conducted at Accel Volt of 10 kV and the magnifications ranging from 100× to 400× (wd = 39 mm). At 400×, the field of view was approximately 255 × 195 µm, allowing the entire compound eye to be imaged along with the surrounding setae. The microscope is housed at the Central Research Support Services (SCAI), University of Córdoba.

Morphometric variables

SM: Mean length of the setae surrounding the compound eye (µm, 400×). Five setae were selected from the periocular region, distributed between the anterior and posterior areas (see Figure 1), and their mean length was calculated. Each seta was measured as a straight-line distance from its base to the distal tip (Figure 1). Preference was given to setae that were as straight as possible. In SEM images, these setae typically appear closely appressed to the cuticle, facilitating measurement (Figure 2).

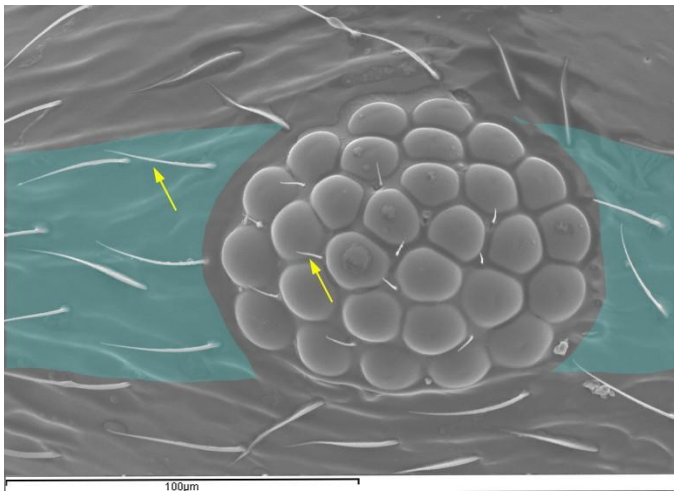

Figure 1. Setae surrounding and interommatidial setae of compound eye of *T. bejaraniensis*.

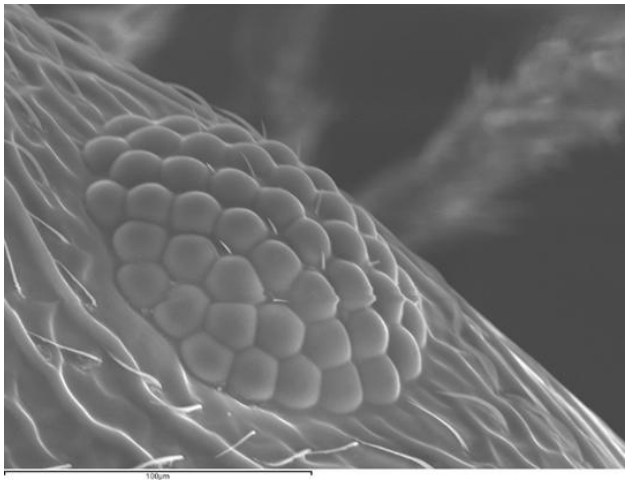

Figure 2. Tangential view of the compound eye where the setae are best seen.

 doi:10.20944/preprints202604.0089.v1

EL: Maximum diameter of the compound eye (μm, 400×), including all structurally visible ommatidia (Figure 3).

OMAT: Total number of ommatidia (400×). A key advantage of SEM is that specimens are coated with a conductive material, making visualization independent of ommatidial pigmentation. This is particularly relevant because, under light microscopy, some ommatidia may lack pigmentation and thus be difficult to discern.

NEIS: Number of interommatidial setae (400×) (Figure 1). Many insect groups possess simple external setae located between ommatidial lenses [18], with diverse functional roles. These structures are also referred to as "interommatidial bristles" or "ommatrichia".

Traditional morphometric variables (μm, all measured at 100×):

HW: Head width, measured in frontal view just above the compound eyes (Figure 4).

HL: Head length. Length of the head capsule excluding mandibles, measured in full-face view as the straight-line distance from the midpoint of the anterior clypeal margin to the midpoint of the posterior head margin.

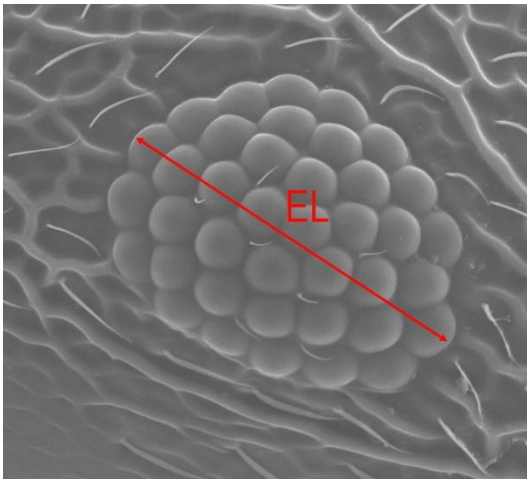

Figure 3. Maximum diameter of the compound eye of *T. curtulus.*

FRS: Distance between the frontal carinae (Figure 4), measured immediately caudal to the posterior intersection points between the frontal carinae and the lamellae dorsal to the torulus [19].

CLI: Distance from the most distal point of the clypeus to the midpoint of the line defined by the FRS measurement (Figure 4).

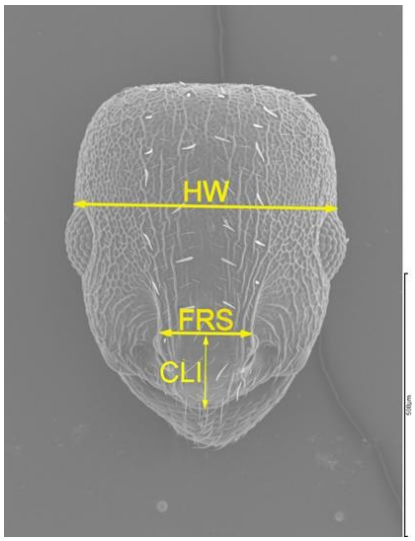

Figure 4. Front view of the head of *T. curtulus* with some of the measured variables.

 doi:10.20944/preprints202604.0089.v1

ML: Mesosoma length (Weber's length). Distance from the caudalmost point of the propodeal lobe to the transition point between the anterior pronotal slope and the anterior propodeal shield, measured in lateral view.

SPST: Distance between the center of the propodeal stigma and the tip of the propodeal spine, measured in lateral view (Figure 5).

SPL: Minimum distance between the center of the propodeal spiracle and the subspinal excavation, measured in lateral view (Figure 5).

Statistical Analysis

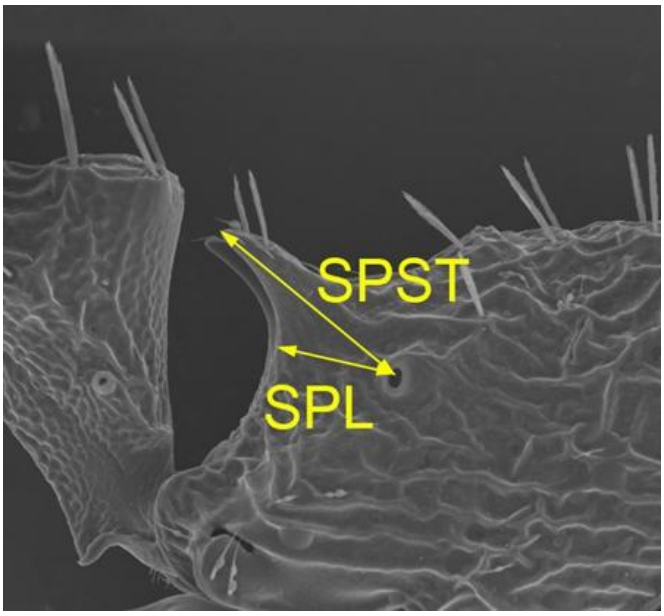

Figure 5. Side view of the spine, with the measured variables.

The discriminative power of the morphometric variables was assessed using multiple analytical approaches. First, a correlation matrix was examined to identify potential redundancy among variables. This was followed by an evaluation of the individual discriminatory capacity of each variable through univariate comparisons. Subsequently, multivariate analyses were performed, including Linear Discriminant Analysis (LDA), with species identity (SPP) treated as the response variable. All species included in this study are currently regarded as valid ("good") species; therefore, the objective of the analyses was not to detect new taxonomic entities [13], but rather to assess whether the selected variables allow for a reliable separation among them. Additional methodological details are provided in the corresponding sections.

All analyses were conducted in the R statistical environment (version 4.5.1, 2025-06-13 ucrt) (R Core Team, 2025. R: A Language and Environment for Statistical Computing. R Foundation for Statistical Computing, Vienna, Austria. https://www.R-project.org/).

3. Results

The analysis was based on a dataset comprising 246 workers, representing 52 nests, 13 populations, and 8 species.

3.1. Correlation Matrix Among Variables

Table 1 shows the Pearson linear correlation coefficients between the variables proposed in this study and the traditional morphometric variables.

OMAT and EL show the highest correlation values, predominantly positive and mostly statistically significant. In contrast, SM tends to be negatively correlated with several variables (CLI, SPST, CS), although with small to moderate effect sizes and, in some cases, lacking statistical

 doi:10.20944/preprints202604.0089.v1

significance. NEIS also exhibits moderate correlations, mainly with SPST and SPL, and weaker associations with ML and CS. A particularly noteworthy finding is the linear relationship between OMAT (number of ommatidia) and CS (head size), indicating that larger head size is associated with a greater number of facets in the compound eyes. Consequently, techniques aimed at minimizing this effect will be applied subsequently.

Table 1. Pearson correlations between SM, OMAT, NEIS, and EL and the remaining variables. Asterisks indicate significance levels: $p < 0.05$ (*), $p < 0.01$ (**), $p < 0.001$ (***). n = 246.

Variable	SM	OMAT	NEIS	EL
CS	-0.165**	0.854***	0.163*	0.915***
FRS	-0.083ns	0.858***	0.097ns	0.899***
CLI	-0.331***	0.131*	0.042ns	0.185**
ML	-0.005ns	0.878***	0.180**	0.895***
SPST	-0.158*	0.473***	0.499***	0.576***
SPL	0.008ns	0.516***	0.450***	0.594***

3.2. Variable-by-Variable Basis

The following sections examine, on a variable-by-variable basis, the potential interspecific differences among the measured traits.

3.2.1. Mean Length of the Setae Surrounding the Compound Eye (SM)

Differences in SM among species were assessed using one-way ANOVA. Due to heterogeneity of variances (Levene's test), a Welch's ANOVA was applied, followed by post hoc comparisons using the Games–Howell test ($\alpha = 0.05$). Significant differences among species were detected (Welch $F(7, 91.57) = 45.43$, $p < 0.001$). The Games–Howell post hoc analysis revealed multiple significant differences (Table 2). Species grouping showed a clear gradient in mean SM values: BEJ exhibited the highest values; TUB and TEB formed a high-intermediate group; UNI and LUT an intermediate group; RAC showed moderate values; and PAR and CUR exhibited the lowest values.

Table 2. Differences among species in SM, OMAT, NEIS, and EL. Values are presented as mean ± standard deviation. Identical letters within each column indicate no significant differences among species according to Games–Howell post hoc comparisons ($\alpha = 0.05$) following a Welch's ANOVA.

SPP	n	SM (µm)	OMAT	NEIS	EL (µm)
BEJ	28	29.07 ± 2.73 a	35.32 ± 3.97 f	8.18 ± 1.68 c	114.96 ± 6.70 e
CUR	38	21.69 ± 2.32 c	40.92 ± 5.15 e	6.76 ± 1.15 d	122.95 ± 7.42 d
LUT	27	25.51 ± 1.77 b	55.04 ± 5.10 d	10.19 ± 1.47 b	141.11 ± 8.08 b
PAR	38	22.36 ± 1.18 c	62.87 ± 4.65 c	9.68 ± 1.45 b	145.87 ± 6.89 b
RAC	44	24.38 ± 1.76 b	55.36 ± 8.24 d	11.75 ± 2.06 a	138.36 ± 11.43 c
TEB	21	26.86 ± 2.64 a	43.76 ± 4.84 e	10.62 ± 1.32 a	124.00 ± 6.16 d
TUB	29	27.61 ± 2.60 a	76.10 ± 8.60 b	8.90 ± 1.61 b	155.72 ± 8.73 a
UNI	21	25.55 ± 1.41 b	89.86 ± 9.03 a	8.90 ± 1.37 b	160.76 ± 9.44 a

3.2.2. Number of Interommatidial Setae (NEIS)

Differences in NEIS among species were assessed using a one-way ANOVA. Due to heterogeneity of variances (Levene's test), a Welch's ANOVA was applied, followed by post hoc comparisons using the Games–Howell test ($\alpha = 0.05$). Significant differences among species were detected (Welch $F(7, 93.51) = 39.30$, $p < 0.001$). The Games–Howell post hoc analysis identified 23 significant pairwise comparisons. Species grouping revealed a clear interspecific gradient: RAC exhibited the highest NEIS values; TEB and LUT formed a high-intermediate group; PAR showed

 doi:10.20944/preprints202604.0089.v1

intermediate values; UNI, TUB, and BEJ formed a low-intermediate group; and CUR exhibited the lowest values.

3.2.3. Number of Ommatidia

Differences in the number of ommatidia per compound eye (OMAT) among species (SPP) were assessed using a one-way Welch's ANOVA. Highly significant differences in OMAT were detected among species. The Welch's ANOVA was significative ($F(7, 92.99) = 211.20$, $p < 0.001$). The Games–Howell post hoc analysis identified 27 significant pairwise comparisons, revealing a pronounced interspecific gradient: UNI exhibited the highest OMAT values, followed by TUB, PAR, RAC, and LUT (the latter two not significantly different from each other), whereas TEB, CUR, and BEJ showed progressively lower values. Overall, these results demonstrate a very strong interspecific differentiation in the number of ommatidia per compound eye.

3.3. Interocular Correlation

3.3.1. Ommatidia

Measuring both eyes of the same specimen under SEM is technically challenging; therefore, only a limited subset of individuals with both eyes measured was available (n = 37 workers). To assess bilateral symmetry in the number of ommatidia per compound eye (OMAT), the two measurements obtained per individual (OMAT and OMAT2) were analyzed.

As laterality (right vs. left eye) was not recorded, directional asymmetry could not be evaluated. Instead, bilateral asymmetry was estimated using the absolute difference between eyes ($|OMAT - OMAT2|$). In addition, Pearson correlation coefficient was calculated between both measurements as indicators of overall bilateral symmetry. Measurements from both eyes showed an extremely high correlation (Pearson $r = 0.996$, $p < 0.001$), indicating strong bilateral symmetry in ommatidial number. The mean absolute difference between eyes was low (1.32 ± 1.27 ommatidia; maximum = 5), representing minimal variation relative to the total number of ommatidia per individual. Overall, these results demonstrate very high bilateral symmetry, although directional asymmetry could not be assessed due to the lack of laterality information.

3.3.2. NEIS

Asymmetry in the number of interommatidial setae (NEIS) was evaluated in individuals with measurements available for both eyes (NEIS and NEIS2; both eyes of the same worker; n = 37). As laterality (right vs. left eye) was not recorded, directional asymmetry could not be assessed. Instead, bilateral asymmetry was estimated using the absolute difference between eyes ($|NEIS - NEIS2|$). To test whether the magnitude of asymmetry differed among species, a one-way Welch's ANOVA was performed. Mean difference in bilateral asymmetry in NEIS was low (1.49 ± 1.37 setae), with a maximum observed difference of 5 setae. No significant differences in asymmetry magnitude were detected among species (Welch ANOVA: $F(5, 7.49) = 0.95$, $p = 0.504$). Overall, these results indicate that, although NEIS exhibits moderate intra-individual variation between eyes, this variation is relatively consistent across species and does not display a significant interspecific pattern.

3.4. Univariate Discriminative Power of the Variables

The discriminative power of the variables was assessed using Linear Discriminant Analysis (LDA) and Random Forest (RF) with 5-fold cross-validation. Random Forest classifiers were implemented using the default settings of the "randomForest" package in R.

As shown in Table 3, OMAT and FRS exhibited the highest classification performance, whereas SM, NEIS, SPL, and CLI showed considerably lower discriminative power.

To remove the effect of body size, each variable was regressed against CS, and the resulting residuals were used in subsequent analyses (Table 4). Thus, the variables primarily reflect variation

 doi:10.20944/preprints202604.0089.v1

in shape and proportions. Discriminative power was assessed using ANOVA effect size (η^2), as well as univariate LDA and Random Forest analyses (RF). After this correction, SPST exhibited the highest discriminative power among species, followed by OMAT and SM, whereas CLI showed very low discriminative ability.

Table 3. Univariate discriminative power of the variables (n=246).

Variable	η^2 (Welch ANOVA)	LDA accuracy	RF accuracy	Ranking
OMAT	0.860	0.505	0.415	1
FRS	0.855	0.511	0.476	2
SPST	0.847	0.435	0.39	3
EL	0.747	0.403	0.325	4
ML	0.728	0.407	0.354	5
SM	0.583	0.374	0.309	6
SPL	0.542	0.309	0.284	7
NEIS	0.511	0.366	0.342	8
CLI	0.191	0.195	0.325	9

Table 4. Values represent the discriminative power among species after removing the effect of body size (CS) through linear regression. Residuals from these regressions were used in the analyses. The ranking is based on the average of η^2, LDA accuracy, and Random Forest accuracy (n=246).

Variable (residual)	η^2	LDA accuracy	RF accuracy	Ranking
SPST	0.875	0.545	0.443	1
OMAT	0.678	0.371	0.284	2
SM	0.561	0.317	0.273	3
FRS	0.546	0.306	0.212	4
NEIS	0.520	0.350	0.366	5
SPL	0.506	0.289	0.227	6
EL	0.490	0.305	0.223	7
ML	0.307	0.321	0.317	8
CLI	0.191	0.118	0.318	9

3.5. Comparison of Interspecific Discrimination at the Individual vs. Nest Level

Morphometric variables were size corrected by linear regression against head size (CS), used as a proxy for body size. For each variable, a linear model was fitted against CS, and the residuals were used as size-independent variables.

Species discrimination was assessed using LDA. Two independent multivariate analyses were performed: one based on individual worker measurements and another on nest-level mean values. In both cases, a forward stepwise procedure was applied, whereby variables were sequentially included if they improved classification accuracy as estimated by 5-fold cross-validation.

For each final model, cross-validated classification accuracy, apparent accuracy, confusion matrix, proportion of discriminant variance explained by LD1 and LD2, and Wilks' λ (with χ^2 approximation) were calculated to assess overall model significance.

 doi:10.20944/preprints202604.0089.v1

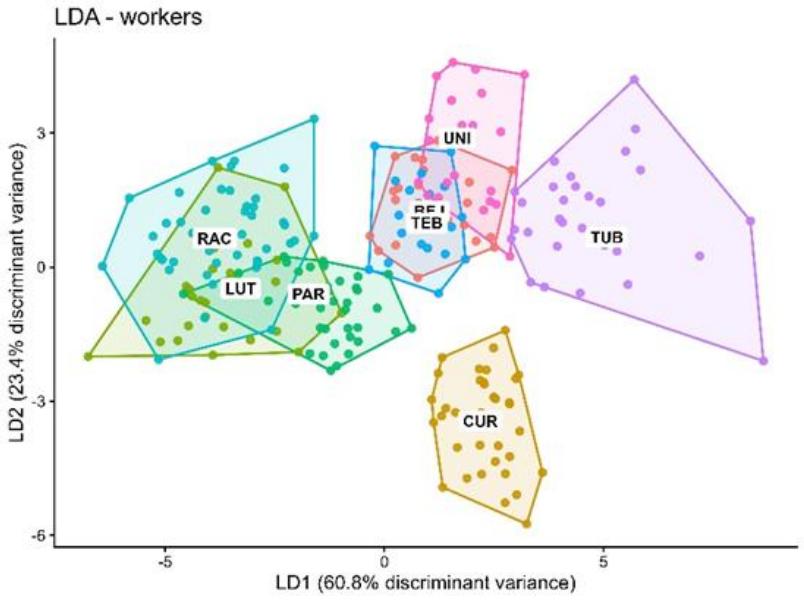

Figure 6.

To specifically evaluate the discriminative power of the variables proposed in this study (SM, OMAT, NEIS, and EL), univariate LDAs were performed using each variable separately as a predictor of species identity. Classification accuracy was estimated using 4-fold cross-validation and compared with that of traditional morphometric variables.

The stepwise procedure applied to individual workers selected seven variables: SPST, OMAT, FRS, SM, SPL, NEIS, and CLI. This model achieved a cross-validated accuracy of 0.871 and an apparent accuracy of 0.894. The first two discriminant axes explained 84.2% of the total discriminant variance (LD1 = 60.8%, LD2 = 23.4%; Figure 6). The model was highly significant (Wilks' $\lambda \approx 0$; $\chi^2 = 4891$; df = 49; $p < 0.001$).

In the nest-level analysis, the stepwise procedure selected four variables: SPST, OMAT, NEIS, and CLI. This model showed slightly higher classification performance (CV accuracy = 0.901; apparent accuracy = 0.923). In this case, LD1 and LD2 explained 76.7% and 18.6% of the discriminant variance, respectively (95.3% cumulative; Figure 7). The model was also highly significant (Wilks' $\lambda \approx 0$; $\chi^2 = 470.3$; df = 28; $p < 0.001$).

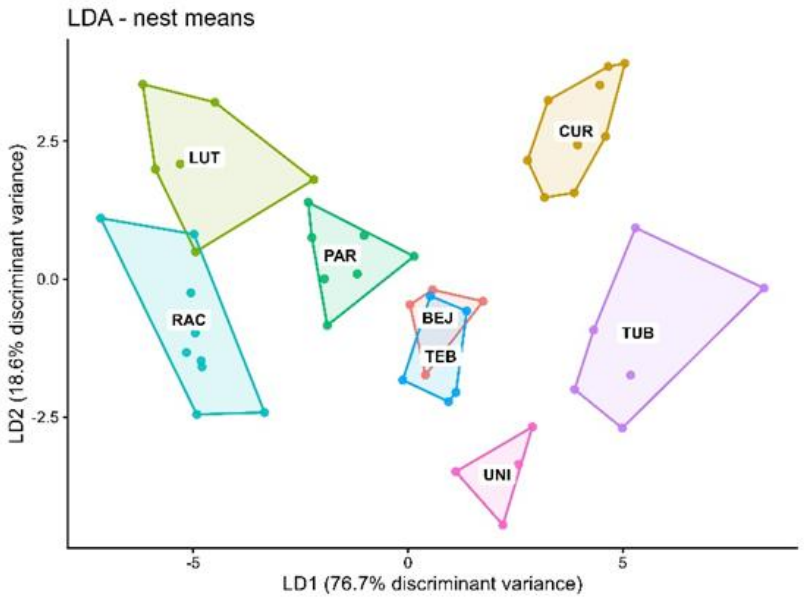

Figure 7. Relative position of the nests on the first two axes of the LDA.

 doi:10.20944/preprints202604.0089.v1

Confusion matrices indicated that most species were correctly classified. In the individual-based analysis, the main misclassifications occurred among LUT, PAR, and RAC, as well as among BEJ, TEB, and UNI, suggesting higher morphological similarity within these groups. In contrast, the nest-based analysis substantially reduced classification errors, with several species classified without error (BEJ, CUR, TEB, and UNI).

Univariate LDA analyses showed that SPST had the highest individual discriminative power (accuracy = 0.62), followed by CS (0.54) and SPL (0.45). Among the variables proposed in this study, SM and NEIS exhibited moderate discriminative ability comparable to several traditional morphometric traits, whereas OMAT and EL showed lower performance when considered in isolation. However, the substantially higher accuracy of multivariate models indicates that species discrimination primarily depends on the combined effect of multiple morphological traits, suggesting that these variables provide complementary information in a multivariate framework.

Overall, these results indicate that using nest-level means yields simpler and slightly more accurate models, suggesting that part of the variation observed at the individual level reflects within-nest variability rather than true interspecific morphological differences.

3.6. Application to the Tebesae Complex

In this case, only *T. bejaraniensis*, *T.* cf. *tebesae*, and *T. curtulus* were compared. To reduce within-nest variation, measurements were averaged at the nest level, retaining species and geographic location as grouping factors.

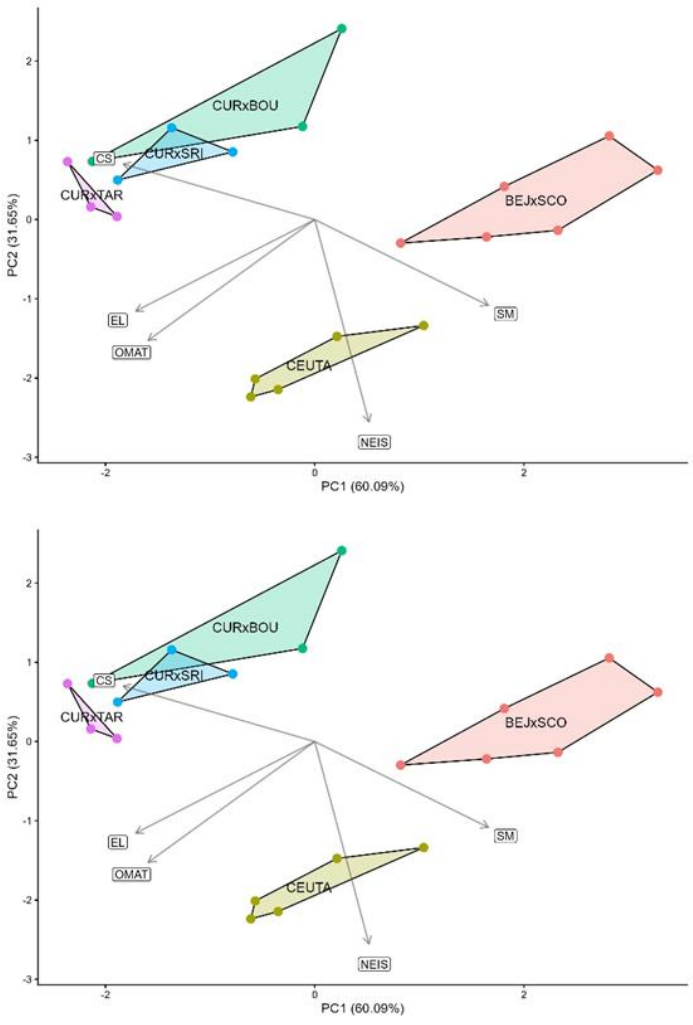

Figure 8. Nests of *T. tebesae* complex on the first two axes of the PCA.

 doi:10.20944/preprints202604.0089.v1

A head size metric (CS) was calculated from head length and width. Subsequently, nest-level means were computed for all morphometric variables. The structure of morphological variation was explored using Principal Component Analysis (PCA), based exclusively on SM, OMAT, EL, NEIS, and CS. Prior to analysis, all variables were centered and standardized. Geographic differentiation was visualized in space defined by the first two principal components. Convex hulls were computed for each geographic group to illustrate the occupied morphospace. In addition, centroids were calculated for each group in the PC1–PC2 plane, and Euclidean distances between centroids were used to quantify morphological divergence. The PCA revealed a strong dimensionality reduction of the dataset. The first principal component (PC1) explained 60.1% of the total variance, while the second component (PC2) explained 31.6%, together accounting for 91.7% of the total variation.

Morphological variables showed a clear correlation structure: EL and OMAT were strongly positively correlated, whereas SM was negatively correlated with head size (CS), indicating that variation in eye morphology and head size contributes substantially to the main morphological gradients. In the PC1–PC2 space, geographic groups formed distinct clusters. BEJxSCO was located at the negative extreme of PC1, whereas CEUTA was primarily separated along PC2. CUR populations clustered in the positive region of PC1 (Figure 8). Centroid distances indicated that CURxBOU and CURxSRI were the most similar populations, whereas CURxTAR showed greater differentiation, particularly relative to CURxBOU. The mean distance among CUR populations in PC1–PC2 space was 1.27, compared to 3.01 between BEJxSCO and TEB.

Multivariate differences in morphospace among species were assessed using permutational multivariate analysis of variance (PERMANOVA), implemented in the adonis2 function (vegan package). Euclidean distances were calculated from the first two PCA axes. Statistical significance was assessed using 9,999 permutations. Homogeneity of group dispersions was tested using a multivariate analogue of Levene's test (betadisper).

PERMANOVA revealed strong differences in morphospace among species ($F = 30.20$, $R^2 = 0.78$, $p < 0.001$). Tests for homogeneity of dispersion were non-significant ($F = 0.40$, $p = 0.68$), indicating that these differences are driven by centroid separation rather than dispersion effects.

4. Discussion

The presence of morphologically cryptic species [20,21] represents a major challenge in insect systematics, including ants. In many groups, evolutionarily distinct lineages may exhibit highly similar external morphology, complicating species delimitation when relying solely on traditional characters observable under light microscopy. This has driven the development of new approaches, particularly the use of high-resolution imaging techniques and the exploration of novel quantitative morphological traits.

In this context, scanning electron microscopy (SEM) has become a particularly valuable tool, enabling detailed examination of microscopic exoskeletal structures that often remain undetected using conventional methods. SEM allows precise characterization of traits such as cuticular microsculpture, setae arrangement, compound eye structure, and sensory morphology.

At the same time, the incorporation of new morphometric variables represents a key strategy for addressing cryptic diversity. While ant taxonomy has traditionally relied on a limited set of linear measurements, the inclusion of additional traits—such as ocular morphology or cephalic geometry—can provide additional discriminatory information, especially when analyzed within a multivariate framework. These findings suggest that ocular morphology represents an underexplored but evolutionarily meaningful axis of morphological differentiation in ants.

Multivariate approaches allow detection of variation patterns that are not evident when characters are analyzed individually. Traits with limited individual discriminatory power may become informative when combined. Thus, the integration of high-resolution imaging (SEM) and new quantitative variables represents a promising strategy for species delimitation in morphologically conserved groups.

 doi:10.20944/preprints202604.0089.v1

The total number of ommatidia remains a relatively underexplored trait. In *Temnothorax*, compound eyes typically contain a low number of ommatidia. In *Temnothorax rugatulus*, values between 45 and 76 ommatidia per eye have been reported, with variation linked to body size [22], and slight interocular asymmetries have been documented in *T. albipennis* [15].

The results show that morphometric approaches effectively discriminate among the studied species. Multivariate LDA models achieved high classification accuracy (≈0.87–0.90), indicating a strong taxonomic signal. Extremely low Wilks' λ values further confirm the robustness of interspecific differentiation.

Nest-level analyses produced simpler and slightly more accurate models than those based on individual workers, suggesting that part of the observed variation at the individual level reflects within-nest variability rather than true interspecific differences. Averaging at the nest level therefore appears to reduce intra-colonial noise and enhance discriminatory signal.

Confusion matrices indicate that most species are clearly separated, although some overlap occurs among certain groups (e.g., LUT, PAR, RAC), suggesting morphological proximity or evolutionary affinities. In contrast, species such as CUR and TUB exhibit more pronounced differentiation.

A key aspect highlighted by this study is the influence of body size on morphometric variables. Size correction reveals that a substantial proportion of the discriminative power is driven by allometric effects. After removing this component through regression against CS, interspecific differences primarily reflect variation in shape and proportions, which are more directly linked to evolutionary and functional divergence.

In this context, the high discriminative power of SPST suggests that propodeal structures carry a strong morphological signal, potentially associated with mechanical or defensive adaptations. Similarly, OMAT retains high discriminative ability even after size correction, reinforcing its value as a functional and ecological trait, likely related to differences in visual reliance among species. The contribution of SM indicates that periocular pilosity also provides relevant information, albeit to a lesser extent.

In contrast, the low discriminative power of CLI suggests that this trait is either relatively conserved or strongly influenced by overall body size, limiting its taxonomic usefulness. These findings highlight the importance of distinguishing between size and shape effects in morphometric studies.

Univariate analyses confirmed that no single variable matches the performance of multivariate models, indicating that species discrimination relies primarily on the combined effect of multiple traits. Among the proposed variables (SM, OMAT, NEIS, EL), SM and NEIS showed performance comparable to traditional traits, while OMAT and EL contribute relevant information when integrated into multivariate models.

Overall, these results demonstrate that incorporating new morphometric traits—particularly those related to ocular morphology—enhances the quantitative characterization of interspecific variation and contributes to more robust species delimitation within a multivariate framework.

5. Conclusions

The results of this study demonstrate that the combination of scanning electron microscopy (SEM) and the use of novel morphometric variables significantly improves species delimitation in morphologically conserved groups such as Temnothorax. Variables related to ocular morphology and cephalic structures provide relevant discriminatory information, particularly when integrated within multivariate frameworks. Correcting for body size is essential to disentangle allometric effects from true shape variation, revealing morphological patterns more directly associated with evolutionary divergence. In this context, traits such as SPST and OMAT exhibit high discriminative power, while other variables contribute complementary information in multivariate models. Moreover, the use of nest-level means enhances model accuracy and reduces the influence of intra-colonial variability, representing a recommended methodological approach in morphometric studies.

 doi:10.20944/preprints202604.0089.v1

Overall, these findings highlight the value of integrating new quantitative morphological approaches with high-resolution imaging techniques to improve the delimitation of cryptic species, providing a robust framework complementary to molecular methods. This approach may be broadly applicable to other morphologically conserved insect groups facing similar taxonomic challenges.

Supplementary Materials: The following supporting information can be downloaded at: https://www.mdpi.com/article/doi/s1, Table S1.

Funding: This research received no external funding.

Data Availability Statement: The raw data supporting the conclusions of this article will be made available by the authors on request.

Acknowledgments: The author thanks the Central Research Support Service (SCAI) of the University of Córdoba for the technical assistance provided in the Microscopy Unit. Thanks to everyone who helped capture the specimens. During the preparation of this manuscript, the authors used ChatGPT (GPT-5.3, OpenAI) to assist in reviewing R scripts and improving the English translation. The authors have reviewed and edited the output and take full responsibility for the content of this publication.

Conflicts of Interest: The authors declare no conflicts of interest.

Appendix A

Table S1.

species.	zone code	zone	province	latitude	longitude	Alt(m)
Temnothorax bejaraniensis	BEJ	Sierra de Córdoba	Córdoba	37.918333	-4.887500	410
Temnothorax cf *tebessae*	TEB-CEU	Ceuta, Spain (N. Africa)	Ceuta	35.913611	-5.370834	65
Temnothorax cutulus	CUR-EST	Los Alcornocales Natural Park	Cádiz	36.084667	-5.533000	390
	CUR-BOU	Bouhachem National Park (N. Africa)	Chefchaouen	35.346830	-5.550360	725
	CUR-SSU	Sierras Subbéticas Natural Park	Córdoba	37.459750	-4.351432	850
Temnothorax luteus	LUT-CAZ	Sierras de Cazorla, Segura y Las Villas Natural Park	Jaen	37.813978	-2.960062	1807
	LUT-SMA	Sierra Mágina Natural Park	Jaen	37.715660	-3.452142	1748
Temnothorax pardoi	PAR-CAZ	Sierras de Cazorla, Segura y Las Villas Natural Park	Jaen	38.318962	-2.578504	1309
	PAR-SGU	PN de la Sierra de Guadarrama Natural Park	Madrid	40.867149	-3.763088	1508
Temnothorax racovitzai	RAC-CAR	Sierra de Cardeña y Montoro Natural Park	Córdoba	38.133328	-4.276874	567
	RAC-SCO	Sierra de Córdoba	Córdoba	37.918333	-4.887500	410
Temnothorax tuberum	TUB	Sierra de Albarracín	Teruel	40.484846	-1.587982	1822
Temnothorax unifasciatus	UNI-SGU	Sierra de Guadarrama National Park	Madrid	40.867149	-3.763088	1508

References

1. Garcia, F.H.; Fischer, G.; Liu, C.; Audisio, T.L.; Alpert, G.D.; Fisher, B.L.; Economo, E.P. X-Ray Microtomography for Ant Taxonomy: An Exploration and Case Study with Two New *Terataner*

 doi:10.20944/preprints202604.0089.v1

(Hymenoptera, Formicidae, Myrmicinae) Species from Madagascar. PLoS One 2017, 12, doi:10.1371/journal.pone.0172641.

2. Friedrich, F.; Matsumura, Y.; Pohl, H.; Bai, M.; Hörnschemeyer, T.; Beutel, R.G. Insect Morphology in the Age of Phylogenomics: Innovative Techniques and Its Future Role in Systematics. Entomol. Sci. 2014, 17.
3. Mensa, F.S.; Di Giulio, A.; Muzzi, M.; Spani, F.; Tromba, G.; Dullin, C. When the Utility of Micro-Computed Tomography Collides with Insect Sample Preparation: An Entomologist User Guide to Solve Post-Processing Issues and Achieve Optimal 3D Models. Applied Sciences (Switzerland) **2022**, 12, doi:10.3390/app12020769.
4. Roháček, J.; Hammel, J.U.; Baranov, V. Christelenkidae, a New Extinct Family Based on a New Taxon from Eocene Baltic Amber (Diptera: Acalyptratae), with X-Ray Synchrotron Microtomography Imaging of Its Structures. Arthropod Syst. Phylogeny *2023*, 81, doi:10.3897/asp.81.e101441.
5. Nelson, L.; Doucet, D.S.; Cook, J.L. Morphology of Cuticular Structures in the Ant Genus *Strumigenys* (Insecta: Hymenoptera: Formicidae). Zoomorphology **2024**, 143, doi:10.1007/s00435-024-00671-6.
6. Birkenfeld, V.; Gorb, S.N.; Krings, W. Mandible Elemental Composition and Mechanical Properties from Distinct Castes of the Leafcutter Ant Atta laevigata (Attini; Formicidae). Interface Focus **2024**, 14, doi:10.1098/rsfs.2023.0048.
7. Wang, C.; Chung, F.Y.; Lin, C.C.; Gibson, J.C.; McGuire, S.; Suarez, A. V.; Billen, J. The Spongiform Tissue in *Strumigenys* Ants Contains Exocrine Glands. Arthropod Struct. Dev. **2023**, 73, doi:10.1016/j.asd.2023.101246.
8. Morris, P. Animal Eyes (Oxford Animal Biology Series)—By Michael F. Land & Dan-Eric Nilsson. Zool. J. Linn. Soc. **2012**, 166, doi:10.1111/j.1096-3642.2012.00849.x.
9. Warrant, E.; Dacke, M. Vision and Visual Navigation in Nocturnal Insects. Annu. Rev. Entomol. **2011**, 56, doi:10.1146/annurev-ento-120709-144852.
10. Agavekar, G.; Hita Garcia, F.; Economo, E.P. Taxonomic Overview of the Hyperdiverse Ant Genus Tetramorium Mayr (Hymenoptera, Formicidae) in India with Descriptions and X-Ray Microtomography of Two New Species from the Andaman Islands. PeerJ **2017**, 5, e3800, doi:10.7717/peerj.3800.
11. Fischer, G.; Hita Garcia, F.; Peters, M.K. Article Taxonomy of the Ant Genus Pheidole Westwood (Hymenoptera: Formicidae) in the Afrotropical Zoogeographic Region: Definition of Species Groups and Systematic Revision of the Pheidole pulchella Group. Zootaxa **2012**, 3232, 1–43.
12. Garcia, F.H.; Fischer, G.; Liu, C.; Audisio, T.L.; Alpert, G.D.; Fisher, B.L.; Economo, E.P. X-Ray Microtomography for Ant Taxonomy: An Exploration and Case Study with Two New Terataner (Hymenoptera, Formicidae, Myrmicinae) Species from Madagascar. PLoS One **2017**, 12, e0172641, doi:10.1371/journal.pone.0172641.
13. Johnson, R.A.; Rutowski, R.L. Color, Activity Period, and Eye Structure in Four Lineages of Ants: Pale, Nocturnal Species Have Evolved Larger Eyes and Larger Facets than Their Dark, Diurnal Congeners. PLoS One **2022**, 17, e0257779, doi:10.1371/journal.pone.0257779.
14. Snelling, R.; Borowiec, M.; Prebus, M. Studies on California Ants: A Review of the Genus Temnothorax (Hymenoptera, Formicidae). Zookeys **2014**, 372, 27–89, doi:10.3897/zookeys.372.6039.
15. Prebus, M.M. Taxonomic Revision of the Temnothorax salvini Clade (Hymenoptera: Formicidae), with a Key to the Clades of New World *Temnothorax*. PeerJ **2021**, 9, e11514, doi:10.7717/peerj.11514.
16. Hunt, E.R.; Dornan, C.; Sendova-Franks, A.B.; Franks, N.R. Asymmetric Ommatidia Count and Behavioural Lateralization in the Ant *Temnothorax albipennis* OPEN. **2018**, 8, 5825, doi:10.1038/s41598-018-23652-4.
17. Cagniant, H.; Espadaler, X. Les Leptothorax, Epimyrma et Chalepoxenus Du Maroc (Hymenoptera: Formicidae). Clé et Catalogue Des Espèces. Annales de la Société entomologique de France (N.S.) **1997**, 33, 259–284, doi: 10.1080/21686351.1997.12277888.
18. Campos, B.B.; Correia, A.O.; Campos, L.A.; Fernandes, J.A.M. Morphology of Interommatidial Sensilla of Discocephalini (Heteroptera: Pentatomidae: Discocephalinae). Arthropod Struct. Dev. **2023**, 72, 101216, doi: 10.1016/j.asd.2022.101216.

 doi:10.20944/preprints202604.0089.v1

19. Seifert, B.; Csösz, S. Temnothorax Crasecundus Sp. n.—A Cryptic Eurocaucasian Ant Species (Hymenoptera, Formicidae) Discovered by Nest Centroid Clustering. Zookeys **2015**, doi:10.3897/zookeys.479.8510.
20. Seifert, B. Cryptic Species in Ants (Hymenoptera: Formicidae) Revisited: We Need a Change in the Alpha-Taxonomic Approach. Myrmecol. News **2009**, 12, 149–166, doi:10.25849/myrmecol.news_012:149.
21. Li, X.; Wiens, J.J. Estimating Global Biodiversity: The Role of Cryptic Insect Species. Syst. Biol. **2023**, 72, 391–403, doi: 10.1093/sysbio/syac069.
22. Ramirez-Esquivel, F.; Leitner, N.E.; Zeil, J.; Narendra, A. The Sensory Arrays of the Ant, Temnothorax rugatulus. Arthropod Struct. Dev. **2017**, 46, 552–563, doi: 10.1016/j.asd.2017.03.005.